JOURNAL OF GUIDANCE, CONTROL, AND DYNAMICS
Vol. 28, No. 6, November–December 2005

Rudder Control Strategies and Force/Feel System Designs in Transport Aircraft

Ronald A. Hess*
University of California, Davis, Davis, California 95616

An analytical investigation of rudder control strategies in transport aircraft is undertaken. The study was motivated by an airline crash in which rudder usage by the pilot might have been a contributing factor. A detailed mathematical model of the human pilot is employed in a computer simulation to examine the closed-loop nature of rudder control strategies. Emphasis is placed on pilot-induced oscillation tendencies. A task suitable for pilot-in-the-loop flight-simulator evaluation of rudder control systems is proposed. A comparison of the pedal force/feel characteristics of three transport aircraft and a military helicopter is provided. The adverse effect that highly nonlinear pedal force/feel system characteristics can have on pilot/vehicle response predictability is demonstrated. A linearity index is defined to quantify the linear force/displacement characteristics of any force/feel system.

Nomenclature

$A_{(-)}$ = gain factors in vehicle transfer functions
$a_{y_{ps}}$ = lateral acceleration at pilot's station, g
C = command input in structural pilot model
E = system error in structural pilot model
$\text{Force}|_{\text{breakout}}$ = minimum force applied to inceptor that overcomes breakout, lbf
$\text{Force}|_{\text{max}}$ = force applied to inceptor that results in maximum control effector (control surface) displacement, lbf
K_{FS} = gain in model of inceptor force/feel system used in structural pilot model
K_{factor} = gain factor in structural pilot model to compensate for gain reduction caused by inceptor threshold nonlinearity
$K_{\dot{m}}$ = gain in vestibular feedback loop in structural pilot model
K_{PF} = gain in proprioceptive feedback loop in structural pilot model
K_p = gain in simplified pilot model
K_{p_ϕ} = gain in simplified pilot model compensation for roll-attitude control
K_r = gain value that defines rudder pedal input in combined use of aileron and rudder in structural pilot model
M = output in structural pilot model
r = vehicle yaw rate
s = Laplace variable, rad/s
T_{PF} = time constant in first-order denominator of proprioceptive feedback transfer function in structural pilot model, s
$T_{(-)}$ = time constant in first-order numerator and denominator factors in vehicle transfer functions, s
v = y-body axis component of velocity of aircraft center of mass, ft/s
x_{ps} = x-body axis coordinate of pilot's station, ft
Y_c = transfer function of vehicle
Y_e = K_e, error compensation element in structural pilot model
Y_{FS} = transfer function of force/feel system in structural pilot model
Y_{NM} = transfer function of pilot neuromuscular system in structural pilot model
Y_{PF} = transfer function of pilot proprioceptive system in structural pilot model
Y_p = transfer function of pilot model
Y_{p_ϕ} = transfer function of pilot model for roll-attitude control
Y_v = mass-normalized lateral-directional stability derivative in vehicle equations of motion, 1/(s)
Y_{δ_r} = mass-normalized lateral-directional stability derivative in vehicle equations of motion (ft/s^2)
y = body-fixed vehicle axis, positive in direction of right (starboard) wing
β = sideslip angle
β_c = command sideslip angle
δ = inceptor output in structural pilot model
δ_a = aileron deflection
δ_{a_c} = input command to aileron actuator
δ_e = elevator deflection
δ_F = force applied to inceptor in structural pilot model
δ_r = rudder deflection
δ_{r_c} = input command to rudder actuator
ζ_{FS} = damping ratio in transfer function describing force/feel system, rad/s
$\zeta_{(-)}$ = damping ratio quadratic factors in transfer functions, rad/s
θ = vehicle pitch attitude
σ = rms value of force applied to inceptor in describing function analysis
τ_0 = time delay in structural pilot model, s
ϕ = vehicle roll attitude
ϕ_c = command roll attitude
ω_{FS} = undamped natural frequency in transfer function describing force/feel system, rad/s
$\omega_{(-)}$ = undamped natural frequency in quadratic factors in transfer functions, rad/s

Received 4 August 2004; presented as Paper 2004-4701 at the AIAA Atmospheric Flight Mechanics Conference, Providence, RI, 16–19 August 2004; revision received 7 October 2004; accepted for publication 13 October 2004.

*Professor, Department of Mechanical and Aeronautical Engineering; rahess@ucdavis.edu. Associate Fellow AIAA.

I. Introduction

RECENT incidents, such as the crash of American Airlines Flight 587 in November 2001, have brought transport pilots' use of rudder control under increased scrutiny.[1–3] This is especially

true in large upsets caused by wake vortex encounters,[4] in which the pilot might employ rudder inputs to augment roll control. With increased air traffic, the introduction of new transport aircraft weighing in excess of 1,000,000 lb, and the constant pressure for reduced aircraft separation, it is apparent that wake vortex encounters and pilot response to these encounters will be of increasing importance to the air-transport community. This study will consider rudder feedback strategies that could be used in such encounters and will demonstrate the effect of pedal force/feel sensitivity on vehicle handling qualities in large disturbance maneuvers.

Section II provides a brief review of rudder control strategies that can be employed by the pilot. Section III discusses models of the human pilot that can be employed in analyzing pilot/vehicle responses in which rudder control plays a part. These models are then exercised in computer simulations of a pair of tasks that could be representative of those employed in large disturbance maneuvers. Section IV provides a comparison of some existing pedal force/feel systems with an emphasis upon the effects of sensitivity. Sections V and VI provide a closing discussion and conclusions, respectively.

II. Rudder Control Strategies for Manual Control

Rudder designs are typically driven by the following general requirements: 1) maintaining zero sideslip in turning flight, that is, overcoming adverse yaw; 2) maintaining or minimizing sideslip in asymmetric power conditions, for example, power loss in multiengine aircraft; 3) maintaining constant sideslip in crosswind landings; and 4) spin recovery. None of these requirements are directed toward use of the rudder in closed-loop tracking control, an activity that will be of central importance in the research to be described.

A. Rudder Feedback Strategies

Reference 5 presents a thorough treatment of various feedback strategies (or surveys) using the rudder as part of an automatic feedback systems, for example, stability augmentation systems. Two strategies of particular interest to this study are 1) feedback of sideslip to rudder, $\beta \rightarrow \delta_r$, and 2) roll attitude to rudder, $\phi \rightarrow \delta_r$, particularly in combination with aileron to rudder, $\phi \rightarrow \delta_r, \delta_a$. Reference 6 provides an analytical and experimental study of lateral-directional manual control. That study involved feedback of roll attitude to aileron, $\phi \rightarrow \delta_a$, and yaw rate to rudder, $r \rightarrow \delta_r$. Some of the results of Refs. 5 and 6 will be revisited in what follows.

The pertinent vehicle transfer functions appropriate for the strategies just outlined can be given in symbolic fashion[5] as sideslip to rudder

$$\frac{\beta}{\delta_r}(s) = \frac{A_\beta\left(1/T_{\beta_1}\right)\left(1/T_{\beta_2}\right)\left(1/T_{\beta_3}\right)}{(1/T_s)(1/T_r)[\varsigma_d, \omega_d]} \tag{1}$$

and roll attitude to rudder

$$\frac{\phi}{\delta_r}(s) = \frac{A_\phi\left(1/T_{\phi_1}\right)\left(1/T_{\phi_2}\right)}{(1/T_s)(1/T_r)[\varsigma_d, \omega_d]} \tag{2}$$

The zero at $s = -1/T_{\phi_2}$ in the numerator of Eq. (2) can be nonminimum phase and possess a relatively small time constant, that is, on the same order as the roll subsidence mode. The roll attitude to aileron transfer function

$$\frac{\phi}{\delta_a}(s) = \frac{A_{\phi_1}[\varsigma_\phi, \omega_\phi]}{(1/T_s)(1/T_r)(\varsigma_d, \omega_d)} \tag{3}$$

Finally, one can consider the possibility that the pilot can employ both aileron and rudder in control of roll attitude. This strategy will be defined here as a combined control strategy. This might occur in a large roll upset where aileron control alone might appear to provide insufficient roll control power. In this case, one can consider

$$\begin{aligned} \phi(s) &= (\phi/\delta_a)(s) \cdot \delta_a(s) + (\phi/\delta_r)(s) \cdot \delta_r(s)|_{\delta_r = K_r \cdot \delta_a} \\ \phi(s) &= (\phi/\delta_a)(s) \cdot \delta_a(s) + (\phi/\delta_r) \cdot K_r \cdot \delta_a(s) \\ (\phi/\delta_a)(s) &= (\phi/\delta_a)(s) + (\phi/\delta_r) \cdot K_r \end{aligned} \tag{4}$$

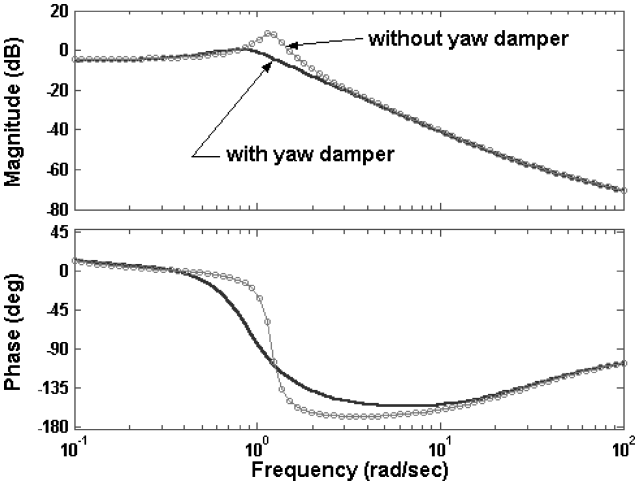

Fig. 1 Bode diagram of (β/δ_r) (s) without and with yaw damper.

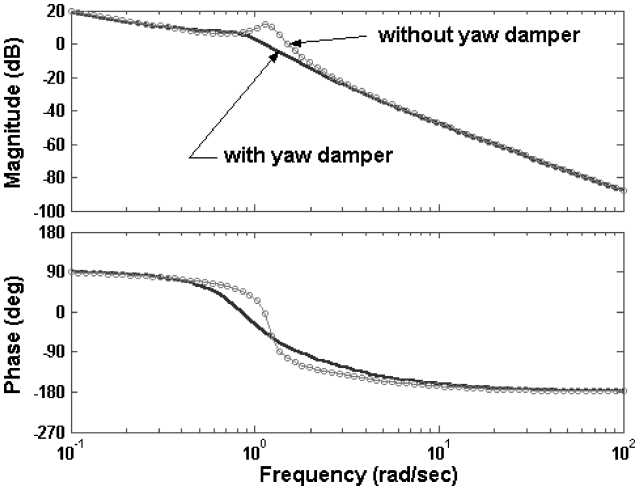

Fig. 2 Bode diagrams of (ϕ/δ_r) (s) without and with yaw damper.

In Eqs. (4) it is assumed that rudder inputs proportional to aileron inputs are commanded with the relation between the two inputs given by $\delta_r = K_r \cdot \delta_a$.

Figures 1 and 2 show the Bode diagrams of the transfer functions in Eqs. (1) and (2) for a generic transport aircraft. This aircraft is the DC-8 vehicle with stability derivatives defined for flight condition "8002" in Ref. 5, corresponding to an airspeed of 468.2 ft/s and an altitude of 15,000 ft. Also shown are the diagrams that result when washed-out yaw rate is fed back to the rudder as a yaw-damper system. The yaw-damper transfer function is given here by

$$\frac{\delta_r}{r}(s) = \frac{1.14(0)}{(0.5)} \text{ rad/(rad/s)} \tag{5}$$

with the gain being chosen as one that increases the damping of the dutch-roll mode form 0.11 to 0.4. The Bode diagrams of Figs. 1 and 2 clearly show the increase in dutch-roll mode damping provided by the yaw damper. Nonminimum phase characteristics are present in Fig. 2, where a 270-deg phase shift from low to high frequencies is evident while the magnitude plot changes from −20 to −40 dB/dec. This right-half plane zero is located at $s = -2.56$.

Figure 3 shows the Bode diagrams for the system of the last of Eqs. (4) for $K_r = 0$, 0.25 0.5, and 0.75. The yaw damper of Eq. (5) is included in each of these systems as are two actuator models for aileron and rudder. These actuator models are given by

$$\frac{\delta_r}{\delta_{r_c}} = \frac{\delta_a}{\delta_{a_c}} = \frac{20^2}{[0.707, 20]} \text{ rad/rad} \tag{6}$$

Employing aileron and rudder deflection limits to be described, $K_r = 0.75$ will produce maximum simultaneous rudder and aileron deflections in this example.

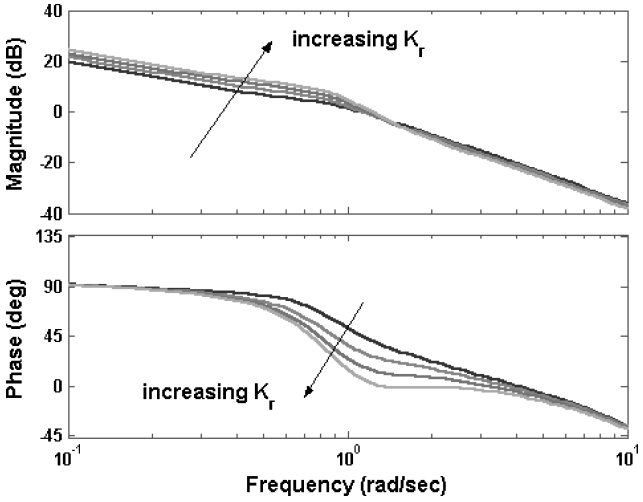

Fig. 3 Bode diagrams of $\phi/\delta_a|_{\delta_r = K_r \cdot \delta_a}(s)$ with yaw damper for $K_r = 0$, 0.25, 0.5, and 0.75, including aileron and rudder actuator models.

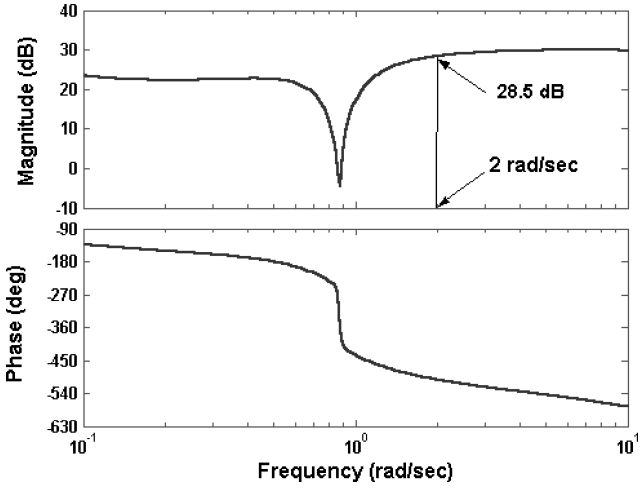

Fig. 4 Bode diagram of $(a_{y_{ps}}/\delta_a)(s)|_{\delta_r = 0.75\delta_a}$.

For frequencies less than 1 rad/s, the Bode diagrams of Fig. 3 show that an increase in roll control power can be obtained with such combined use of rudder and aileron. In the case of $K_r = 0.75$, the increase is approximately a factor of 1.7. In addition, the magnitude and phase curves in this low-frequency range show the K/s-like characteristics long associated with desirable handling qualities (180 deg should be subtracted from the phase curves to account for the sign definitions of positive rudder and aileron). The same cannot be said for larger values of K_r, however, in which phase lags beyond -90 deg appear at frequencies well below the break frequency of a first-order lag appearing approximately 1 rad/s.

B. Handling Qualities Implications of Combined Control

If manual control of roll attitude through combined use of aileron and rudder is attempted, the resulting lateral acceleration at the pilot's station a_{ps} is also pertinent to a discussion of handling qualities. The lateral acceleration to aileron transfer function can be approximated as[5]

$$\left(a_{y_{ps}}/\delta_a\right)(s) \approx Y_v(v/\delta_a)(s)|_{\delta_r = K_r\delta_a} + Y_{\delta_r} \cdot K_r + x_{ps}(\dot{r}/\delta_a)(s)|_{\delta_r = K_r\delta_a} \quad (7)$$

Figure 4 shows the Bode diagram of the transfer function of Eq. (7) for the example vehicle. Here the yaw damper and rudder actuator are included, and $K_r = 0.75$. Figure 4 indicates that if a sinusoidal aileron input of $\delta_a(t) = 20\sin(2t)$ deg with an associated $\delta_r(t) = (15)\sin(2t)$ deg is applied, the resulting amplitude of the sinusoidal lateral acceleration at the pilot's station will be approximately 9.2 ft/s^2 or 0.29 g.

III. Pilot Models for Computer Simulation

A. Introduction

Fundamental manual control theory states that the pilot will provide whatever compensation is necessary to yield an open-loop pilot/vehicle transfer function that resembles K/s in the region of the open-loop crossover frequency.[7] This representation has been referred to as the crossover model of the human pilot and can be represented as

$$Y_p Y_c \approx \omega_c e^{-\tau_e s}/s \quad (8)$$

Also in Eq. (8), ω_c represents the crossover frequency, and τ_e represents an effective delay. The latter encompasses transport delays in the human central nervous system, delays that approximate the higher-frequency human neuromotor dynamics, and higher-frequency vehicle dynamics that might be omitted from Y_c. In what follows, two different tasks and feedback strategies will be examined. First, combined use of aileron and rudder will be examined (including no rudder usage). This strategy might be employed by the pilot in attempting rapid roll-attitude recovery from an upset such as an encounter with a trailing vortex from a lead aircraft. Second, the use of aileron to control roll attitude and rudder to control sideslip will be treated. This strategy might be employed by the pilot in attempting to maintain a desired heading in a crosswind with wings level.

B. Pilot Model for Single-Axis Tracking

To create a realistic computer simulation of the pilot/vehicle system, a more complete pilot model than that implied by Eq. (8) is obviously needed. This will be accomplished by using the structural model of the human pilot.[7] Figure 5 shows the structural pilot/vehicle model appropriate for single-axis tracking of roll attitude, here with aileron inputs, alone. Thus, in Fig. 5, $C \equiv \phi_c$, $M \equiv \phi$, and $\delta \equiv \delta_w$, the displacement of the wheel (output of the wheel force/feel system). Referring to Fig. 5, the following pilot model elements can be given:

1. Visual Gain $Y_e = K_e$

The value of this gain is application dependent and is selected to yield a desired open-loop crossover frequency.[8]

2. Time Delay τ_0

This delay is selected as 0.2 s and models human delay sources exclusive of those associated with neuromuscular system operation.

3. Neuromuscular System Dynamics

These dynamics are modeled as

$$Y_{NM} = \frac{10^2}{s^2 + 2(0.707)10s + 10^2} \quad (9)$$

and represent the actuation dynamics of the particular limb effecting control, for example, arm in wheel motion and leg in pedal motion.

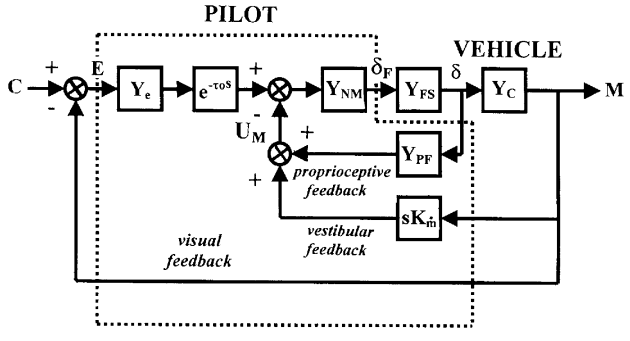

Fig. 5 Structural model of the human pilot.

4. Proprioceptive System Dynamics

In the particular tasks to be discussed, these dynamics are modeled as

$$Y_{\mathrm{PF}} = \frac{K_{\mathrm{PF}}}{(s + 1/T_{\mathrm{PF}})} \tag{10}$$

This form is appropriate for the transfer functions whose Bode diagrams are shown in Fig. 3 because the pole in proprioceptive feedback dynamics will create a zero in the pilot transfer function located as $s = -1/T_{\mathrm{PF}}$.

5. Vestibular System Dynamics

For simplicity, no continuous vestibular feedback will be considered in the model, that is, $K_{\dot{m}} = 0$.

6. Force/Feel System Dynamics

The dynamics of the force/feel system(s) will be of the form

$$Y_{\mathrm{FS}}(s) = \frac{K_{\mathrm{FS}} \cdot \omega_{\mathrm{FS}}^2}{s^2 + 2\varsigma_{\mathrm{FS}}\omega_{\mathrm{FS}}s + \omega_{\mathrm{FS}}^2} \text{ displacement/lbf} \tag{11}$$

C. Modeling Effects of Control Sensitivity

Control sensitivity, or its reciprocal, force gradient, is one of the more important force/feel system parameters as concerns handling qualities and particularly pilot-induced oscillation (PIO) susceptibility. Unfortunately, the manner in which the gain K_{PF} is chosen in the structural model removes all control sensitivity effects.[8] An approximate means of estimating the effects of control sensitivity can, however, be proposed. This approach is based upon the ratio of maximum force to breakout force in the force/feel system, where "maximum force" refers to the force associated with maximum control surface deflection.

Figure 6 shows the structural model for a particular application (here roll attitude to aileron control). An approximation to the control force inputs can be obtained, as follows. The gain value immediately following the "neuromuscular system dynamics" block in Fig. 6 (gain 1) is defined as

$$K_{\mathrm{force}} = \frac{\text{inceptor force for max effector deflection}}{\text{max effector deflection}} \tag{12}$$

(In what follows, "inceptor" refers to the cockpit controller, e.g., wheel or pedal.) A nonlinear threshold element follows gain 1 in Fig. 6 and represents the breakout characteristics of the inceptor. Because of this gain element, the inceptor breakout limits can be directly expressed in terms of a breakout force. The gain following the threshold element (gain 2) is the reciprocal of the gain in Eq. (12). The inceptor displacement is calculated from the output of the force/feel system dynamics through a simple unit conversion defined as

$$K_{\mathrm{displacement}} = \frac{\text{max inceptor displacement}}{\text{max effector deflection}} \tag{13}$$

In terms of a Gaussian input describing function,[9] the threshold element in the force/feel system is equivalent to a gain reduction in the forward path of the loop closed around the pilot's neuromuscular system and the inceptor force/feel system. This reduced gain can be approximated as

$$K_{\mathrm{threshold}} \approx 1 - \frac{\mathrm{Force}|_{\mathrm{breakout}}}{\mathrm{Force}|_{\mathrm{max}}} = \frac{\mathrm{Force}|_{\mathrm{max}} - \mathrm{Force}|_{\mathrm{breakout}}}{\mathrm{Force}|_{\mathrm{max}}} \tag{14}$$

[In Eq. (14), it is assumed that $\sqrt{(2\sigma)}$ for the Gaussian input to the nonlinearity is equal to $\mathrm{Force}|_{\mathrm{max}}$.] To model the pilot's attempt to compensate for the gain reduction as a result of the nonlinearity, the gains K_e and K_{PF} are multiplied by a factor equal to the reciprocal of $K_{\mathrm{threshold}}$ in the computer simulation. This multiplying factor, referred to as K_{factor}, is thus defined as follows:

$$K_{\mathrm{factor}} = \frac{\mathrm{Force}|_{\mathrm{max}}}{\mathrm{Force}|_{\mathrm{max}} - \mathrm{Force}|_{\mathrm{breakout}}} \tag{15}$$

In Eqs. (14) and (15), $\mathrm{Force}|_{\mathrm{max}}$ corresponds to inceptor force corresponding to maximum effector deflection in Eq. (12). Thus, if in Eq. (15), $\mathrm{Force}|_{\mathrm{max}} = 25$ lbf and $\mathrm{Force}|_{\mathrm{breakout}} = 5$ lbf, $K_{\mathrm{factor}} = 25/20 = 1.25$, and the gains K_e and K_{PF} are multiplied by 1.25. Because the pilot/vehicle transfer function in any modeling application will have finite stability margins, K_{factor} can induce closed-loop instability if the $\mathrm{Force}|_{\mathrm{breakout}}$ is of the same order of magnitude as $\mathrm{Force}|_{\mathrm{max}}$. If no breakout force is in evidence, however, the procedure just described will *not* accommodate the effects of control sensitivity. The changes in open-loop pilot/vehicle dynamics that accompany the increases in K_e and K_{PF} just described are qualitatively similar to those that have been measured in experiment. For example, Ref. 10 demonstrates that increased neuromuscular "tension" results in significant decrements in the effective neuromuscular time constant $(2\zeta/\omega_n)$ defined in terms of the damping ratio and undamped natural frequency of the closed-loop neuromuscular system. Qualitatively similar results occur with increases in K_e and K_{PF} in the structural pilot model. This is demonstrated in Fig. 7, where the Bode diagrams show a decrement in $2\zeta/\omega_n$ when K_e and K_{PF} are increased (here by a factor of 1.3).

D. Pilot Model for Combined Aileron and Rudder Inputs

For combined use of aileron and rudder, a more complex model than that of Fig. 5 must be employed. The hypothesized model is shown in Fig. 8. Here, the block labeled "structural model for ϕ-loop" is essentially the model of Fig. 5. It is hypothesized that the command to the pedals is obtained from the input signal to the neuromuscular system for the pilot's arm. The specific parameters for the various elements in Fig. 8 can now be given.

1. Proprioceptive Dynamics

Referring to Fig. 3, one sees that the pilot would be required to generate first-order lead with a reciprocal time constant on the order 1/s (the approximate location of the dutch-roll poles with the yaw damper in place). Thus, in its simplest form, the pilot equalization

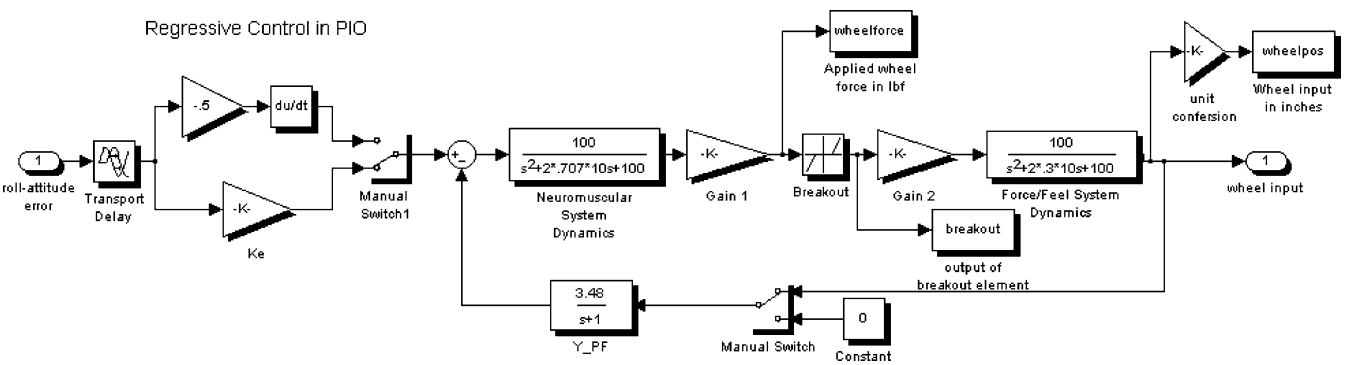

Fig. 6 Structural pilot model for roll attitude to aileron control.

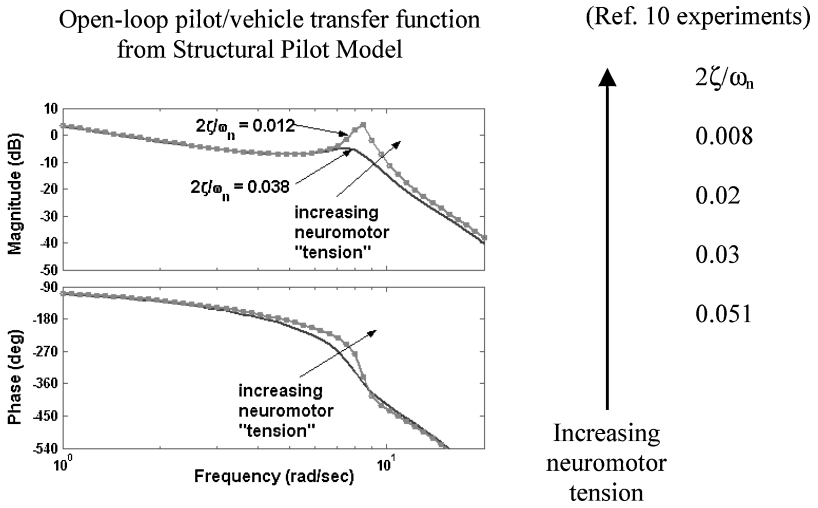

Fig. 7 Qualitative comparison of effect of increased gain in neuromuscular feedback loop of structural model with results from experiment.

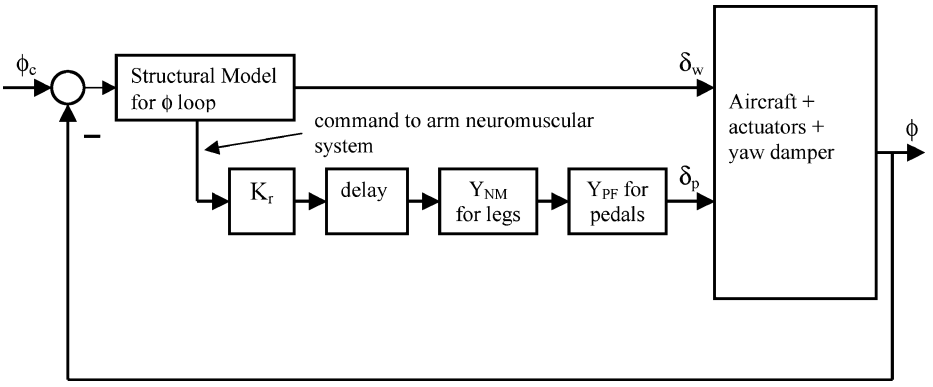

Fig. 8 Pilot/vehicle system for coordinated use of aileron and rudder.

would be

$$Y_{p_\phi} \approx K_{p_\phi}(s+1) \tag{16}$$

Thus, in Eq. (10), $1/T_{\mathrm{PF}} = 1/\mathrm{s}$. The parameter K_{PF} is chosen as the value that yields a minimum damping ratio of 0.15 for any poles of the transfer function resulting when only the proprioceptive loop of Fig. 5 is closed.[8] The form of Eq. (16) would be invariant with K_r values, because, with the exception of an increase in gain, the form of the various vehicle transfer functions in Fig. 3 varies only in phase lag. This fact does not bode well for closed-loop system stability at larger values of K_r.

2. Neuromuscular Dynamics

Y_{NM} will be as given in Eq. (9) for both arm and legs.

3. Force/Feel System Dynamics

Y_{FS} for the wheel and pedals will be given by

$$Y_{\mathrm{FS}}|_{\mathrm{wheel}} = \frac{15 \times 10^2}{s^2 + 2(0.3)10s + 10^2} \text{ wheel deflection/lbf} \tag{17}$$

$$Y_{\mathrm{FS}}|_{\mathrm{pedal}} = \frac{65 \times 20^2}{s^2 + 2(0.3)20s + 20^2} \text{ pedal deflection/lbf} \tag{18}$$

For the wheel, full deflection corresponds to 80-deg wheel rotation and 20-deg aileron deflection. For the pedal, full deflection corresponds to 1.5-in. pedal deflection and 15-deg rudder deflection. The ratio of maximum rudder deflection to maximum aileron deflection was employed in Sec. II in the selection of the maximum value of K_r. The $K_{\max}$ for the aileron is 15 lbf and 65 lbf for the pedals. The breakout forces for the wheel and pedal are as follows: wheel, 2 lbf; pedal, 13 lbf.

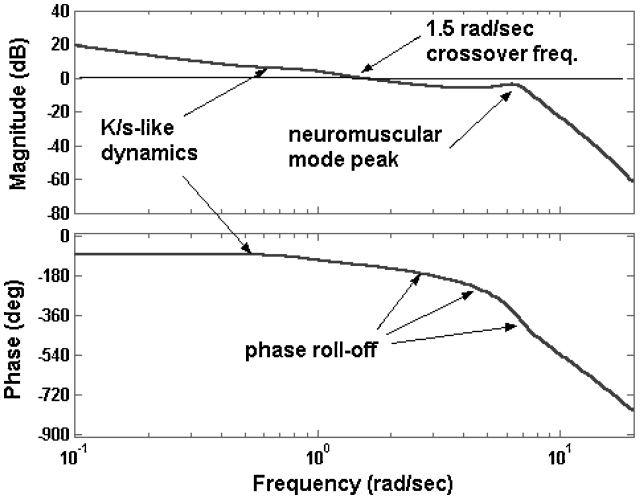

Fig. 9 Bode diagram of open-loop pilot/vehicle transfer function with $K_r = 0$.

4. Delay

The "delay" in Fig. 8 is identical to that in the pilot model of Fig. 5, 0.2 s.

5. Actuator Dynamics and Limits

The dynamics of the actuators for both rudder and aileron have been given in Eq. (6). The amplitude and rate limits of these actuators are as follows: aileron—amplitude limit = ±20 deg, rate limit = ±45 deg/s; rudder—amplitude limit = ±15 deg, rate limit = ±60 deg/s. Figure 9 shows the resulting Bode diagram for

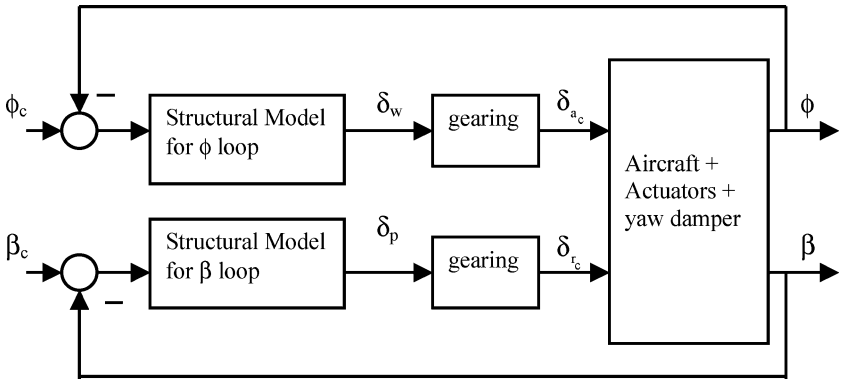

Fig. 10 Pilot/vehicle system for roll attitude to aileron and sideslip to rudder.

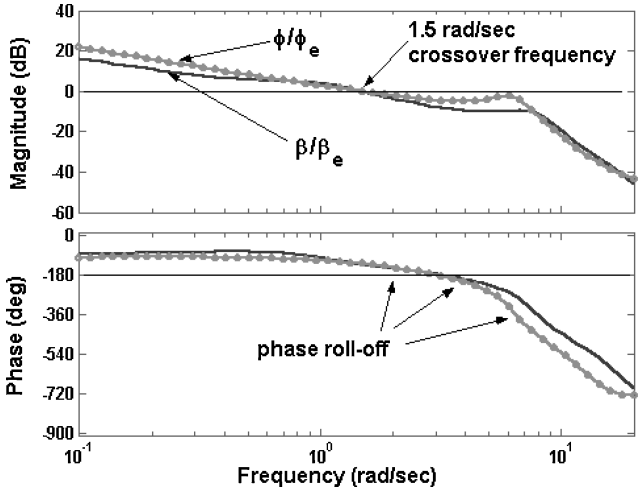

Fig. 11 Bode diagrams of open-loop pilot/vehicle transfer functions for roll and sideslip loops.

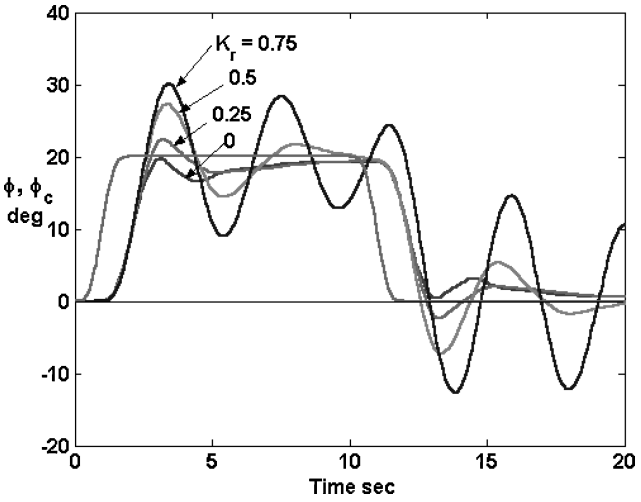

Fig. 12 Computer simulation of pilot/vehicle system with aileron input alone ($K_r = 0$) and with coordinated aileron and rudder inputs ($K_r = 0.25$, 0.50, and 0.75).

the open-loop pilot/vehicle transfer function with $K_r = 0$ and with K_{factor} set to unity. The diagram is very similar in form to measured pilot/vehicle transfer functions in single-axis tracking tasks.[10]

E. Pilot Model for Control of Roll Attitude with Aileron and Sideslip with Rudder

The hypothesized model for control of roll attitude with aileron and sideslip with rudder is shown in Fig. 10. Here, separate structural pilot models are employed in each loop. Based on the ϕ/δ_a and β/δ_r transfer functions for this flight condition, the pilot would again be required to generate first-order lead in each loop, with a reciprocal time constant on the order 1/s for each. Because two loops are assumed to be closed by the pilot, an iterative procedure is employed to determine the forms of the pilot models for each loop. As in the study with combined aileron and rudder, the general form of Y_{PF} for both loops is as given in Eq. (10). First, the rudder loop is left open, and appropriate structural model pilot dynamics are selected for the aileron loop. After selection of the aileron-loop pilot model, this control loop is closed, and appropriate structural model pilot dynamics are selected for the sideslip loop. The procedure is repeated until no significant changes in the pilot models occur. Figure 11 shows the Bode diagrams of the open-loop pilot/vehicle transfer functions for each loop, with the remaining loop closed. This form of the pilot/vehicle system could be employed in modeling coordinated turns, but here attention will be focused on a task involving wings-level sideslip captures.

F. Piloting Tasks for Computer Simulation

1. Task 1: Large Roll-Attitude Change

The command roll attitude will be a filtered step command in which the pilot uses aileron alone with no pedal inputs. Next, the same roll-attitude command will be used, but this time the pilot model will be employing combined aileron and pedal inputs. In this second scenario, various K_r values will be chosen with the largest representing the ratio of maximum displacements of aileron and rudder, that is, $K_r = 0.75$. The crossover frequency for the roll-attitude loop with no rudder inputs will be chosen as 1.5 rad/s. The gain $Y_e = K_e$ selected for $K_r = 0$ will remain unchanged for the remaining K_r values. K_{factor} for the aileron loop is, from Eq. (15), $K_{\text{factor}} = 15/13 = 1.15$. For the rudder loop, $K_{\text{factor}} = 65/52 = 1.25$. Figure 12 shows the simulation results. When the maximum $K_r = 0.75$ is employed, the closed-loop pilot/vehicle system is nearly unstable, with an oscillatory frequency of 1.5 rad/s.

The results indicate that the dutch-roll mode has been excited with the manual loop closures examined here. With $K_r = 0$ and 0.25, the closed-loop system responds well. The aileron and rudder inputs for each $K_r = 0$ are shown in Fig. 13. Note the amplitude limiting of the rudder. The residual rudder motion with $K_r = 0$ is attributable to the action of the yaw damper. Significant aileron rate limiting also occurs in this task. Figure 14 compares aileron and rudder inputs and rates for $K_r = 0.5$. Amplitude limiting of the aileron is again in evidence. As with $K_r = 0$, significant aileron rate limiting again occurs in this task. Figure 15 compares the lateral acceleration at the pilot's station for the two K_r values. Note that for $K_r = 0.5$, the lateral acceleration can reach 0.3 g.

Figure 16 shows the lateral acceleration at the pilot's station that occurs for $K_r = 0.35$ with nominal and high rudder sensitivity, here defined as $K|_{\text{force}} = 32$ lbf and $K|_{\text{breakout}} = 22$ lbf. This yields $K_{\text{factor}} = 32/10 = 3.2$ for the rudder channel. The increased rudder sensitivity has significantly increased the maximum values of a_{ps}.

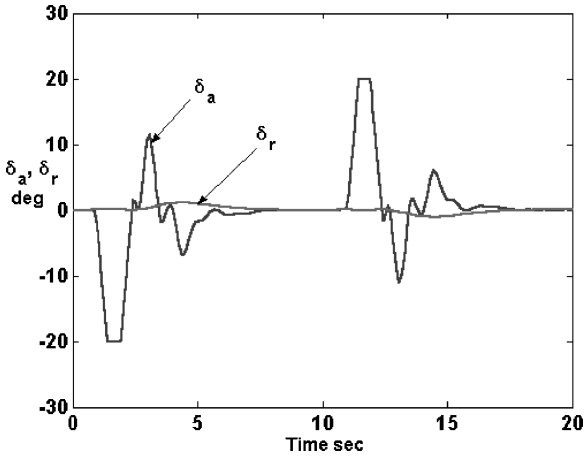

Fig. 13 Aileron and rudder inputs for tracking of Fig. 12 for $K_r = 0$.

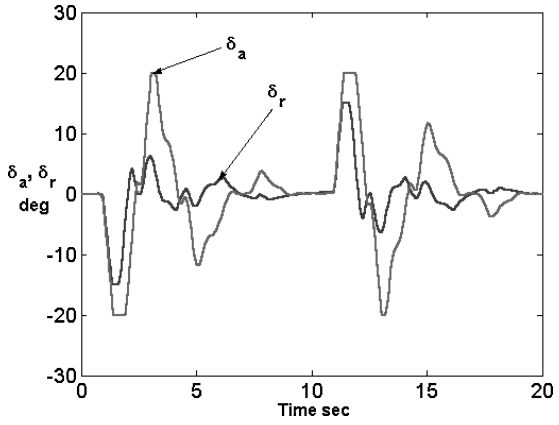

Fig. 14 Aileron and rudder inputs for tracking of Fig. 12 for $K_r = 0.5$.

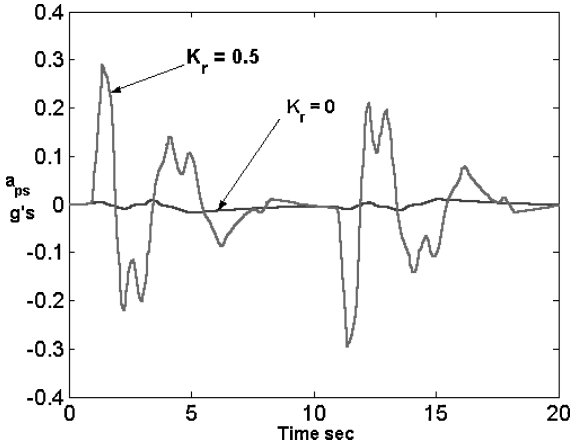

Fig. 15 Lateral acceleration at the pilot's station for tracking of Fig. 12 for $K_r = 0$ and $K_r = 0.5$.

The issue of whether a pilot would coordinate rudder with aileron as was done in the computer simulation just discussed is open to question. Obviously continuous high-gain coordination is detrimental to tracking performance and stability. It is possible, however, that a highly sensitive pedal force/feel system might induce pilot activity of this nature. In addition, the large lateral accelerations that are predicted to develop could precipitate a PIO. Indeed, this scenario was suggested by the author as part of an investigation of the crash of American Airlines Flight 587 (Ref. 11). A PIO can be precipitated in the computer simulation just discussed by forcing the pilot model to adopt so-called "regressive" tracking behavior as discussed in Ref. 10. In this behavior, the pilot is hypothesized

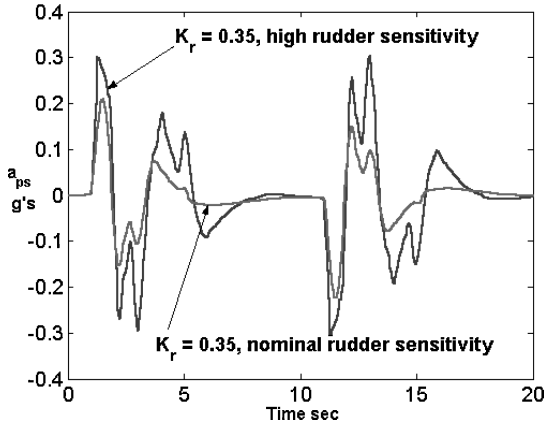

Fig. 16 Lateral acceleration at the pilot's station for tracking of Fig. 12 for $K_r = 0.35$ with nominal and high rudder sensitivity.

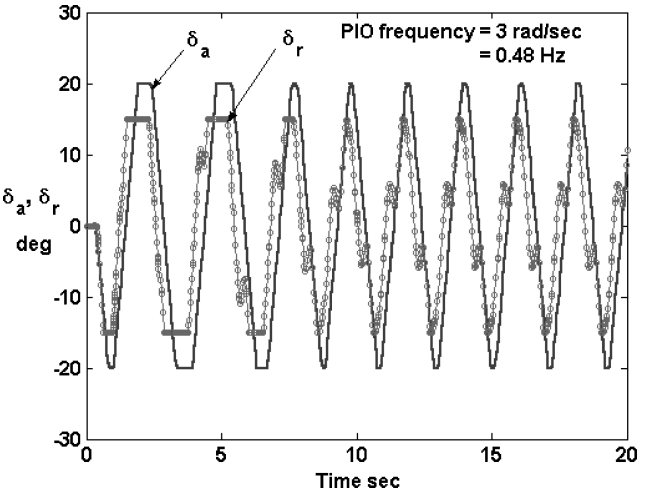

Fig. 17 Rudder and aileron inputs in simulated PIO with pilot model adopting regressive behavior.

to use roll rate rather than roll attitude as the fundamental visual cue. In addition, proprioceptive cues are assumed to be ignored. Figure 17 shows aileron and rudder inputs demonstrating the oscillatory vehicle responses that develop with this regressive behavior. Here the pilot gain was selected as the minimum value that would yield the oscillatory behavior. The aileron and rudder inputs indicate that amplitude and rate saturation of these devices is occurring. The frequency of the PIO is approximately 3.0 rad/s (0.48 Hz), a factor of two greater than the oscillatory frequency evident in Fig. 12 for $K_r = 0.75$. This simulation does not imply that the vehicle chosen for study is PIO prone. Rather, an overly sensitive pedal force/feel system (low force gradient) could precipitate a PIO in a sudden upset by inducing large lateral accelerations at the pilot's station.

2. *Task 2: Wings-Level Sideslip Captures*

In this task, demanding discrete sideslip captures are required while attempting to maintain a wings-level attitude. The command roll attitude for this task will be zero, with the sideslip command consisting of a filtered doublet alternating between ± 6 deg in amplitude. One physical interpretation for this input would be the aircraft experiencing a 30-kn wind that alternates between ± 30 deg from the aircraft's initial heading. Here each alternating pulse lasts approximately 6 s.

As was the case in Fig. 9, K/s-like dynamics are evident, and a common crossover frequency of 1.5 rad/s is chosen. Once, again, this crossover frequency was created with $K_{\text{factor}} = 1$ in each loop. Figure 18 shows the responses in roll attitude and sideslip. Note the significant roll-attitude excursions from the desired wings-level

condition. This is attributable to the significant amount of sideslip to roll coupling that exits, that is, the C_{l_β} effect. Figure 19 shows the aileron and rudder inputs. Minor rudder rate limiting was in evidence in this task. The maximum lateral acceleration at the pilot's station was approximately 0.35 g.

Increasing the sensitivity of the rudder system to the high level of the preceding simulation resulted in incipient instability in the pilot/vehicle system. This is likely to serve as a triggering event for a PIO. Creating regressive behavior in the pilot model in both the roll and sideslip channels leads to a PIO very similar in form to that of Fig. 17. The PIO frequency is approximately 2.9 rad/s or 0.46 Hz with significant amplitude and rate limiting in evidence.

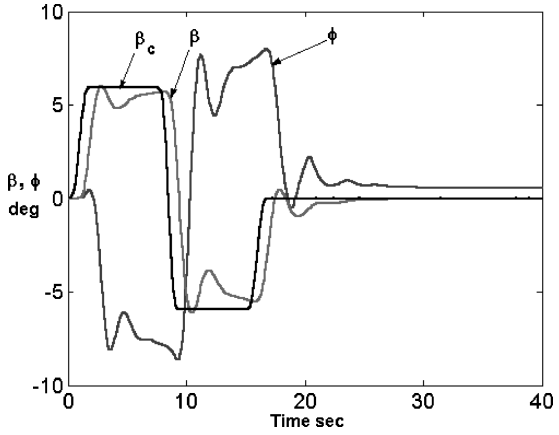

Fig. 18 Computer simulation of pilot/vehicle system to alternating sideslip commands.

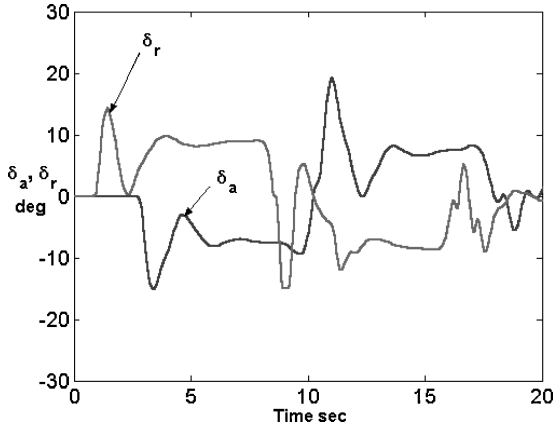

Fig. 19 Aileron and rudder inputs for tracking of Fig. 18.

G. Discussion

Compared to those for wheel and column, pedal force/feel system designs have received little attention in the literature.[12] However, recent accidents such as American Airlines Flight 587, and other rudder-related incidents with transport aircraft,[13] have uncovered a need for firm design requirements for these systems. Given the inherent dangers of flight testing in which the possibility of excessive vertical stabilizer loading can easily occur, it would appear that ground-based flight simulators offer the most practical means for delineating acceptable force/feel characteristics. It is essential in defining the tasks that would be performed in such investigations that the recommendations of Ref. 14 be recalled. Specifically, any tasks selected for discerning the PIO susceptibility of force/feel system characteristics need to be sufficiently challenging and aggressive. The wings-level sideslip capture task exercised herein via computer simulation can serve as one such task.

With one exception, the pilot-modeling assumptions and pilot-parameter selections that have been described are based on a well-documented model of the human pilot acting in compensatory (error-correcting) fashion. The single exception is the model for accommodating the effects of breakout nonlinearity in the cockpit inceptor. The approach espoused here, however, does create closed-loop changes in the pilot's neuromuscular dynamics that have been experimentally shown to accompany increased neuromuscular tension.

IV. Pedal Force/Feel System Comparison

At this juncture, a comparison of some representative aircraft pedal force/feel systems is in order. The plots of Figs. 20–22 represent a comparison of three transport aircraft pedal force/feel systems with that of a helicopter. These vehicles will be identified here as H (helicopter), TA1, TA2, and TA3 (transport aircraft 1, 2, and 3). Vehicle H is a medium-size utility/transport vehicle used by the U.S. Army. Vehicles TA1–TA3 are aircraft of comparable size and passenger-carrying capability (approximately 250 passengers) and are of similar size and configuration to the aircraft involved in the American Airlines Flight 587 accident. Vehicles TA1 and TA3 are currently in service with a number of airlines, worldwide. Vehicles TA2 and TA3 were produced by the same manufacturer, with TA2 being the immediate predecessor of TA3. Indeed, vehicle TA3 is very similar in size, weight, and configuration to TA2. Figures 20–22 involve straight-line approximations to the force/displacement characteristics with full-control movement, with no "cable stretch" involved. As opposed to the data for vehicles H and TA3, the data for vehicles TA1 and TA2 were obtained from tabular data that did not give specific force/feel characteristics within the breakout area.

As used here, "maximum force" is defined as the pedal force that yields a maximum pedal displacement without inducing cable stretch in the mechanical system. As will be seen, larger forces can be applied to the force/feel system. Finally, the force/feel characteristics for the pedal system of TA3 are a function of airspeed. Indeed,

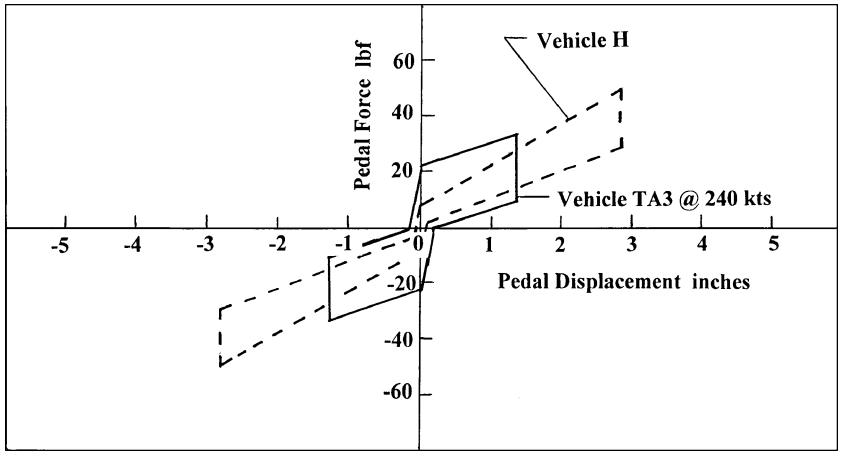

Fig. 20 Pedal force/feel system comparison between vehicle TA3 at 240 kn and vehicle H.

this is the reason for associating the particular data for this vehicle with the 240-kn airspeed. This is not the case for vehicles H, TA1, and TA2, where the force/feel pedal characteristics are invariant with airspeed. The rudder systems for vehicles TA1 and TA2 are referred to as "ratio" systems, whereas that for the TA3 is referred to as a "variable-stop" system.

The reason for choosing the helicopter for a benchmark case is that this vehicle is capable of performing tasks in which precise heading/yaw-rate control is possible with pedal inputs.[15] These tasks consist of hovering turns, pirouettes, lateral repositions, and sidesteps in which heading performance requirements are defined in quantitative fashion.[16] Of course, desirable handling qualities and task performance depend on more than just the characteristics of the force/feel system. However, acceptable force/feel system characteristics constitute a necessary condition for achieving these. Thus, the nature of the pedal force/feel system on vehicle H is of more than just passing interest.

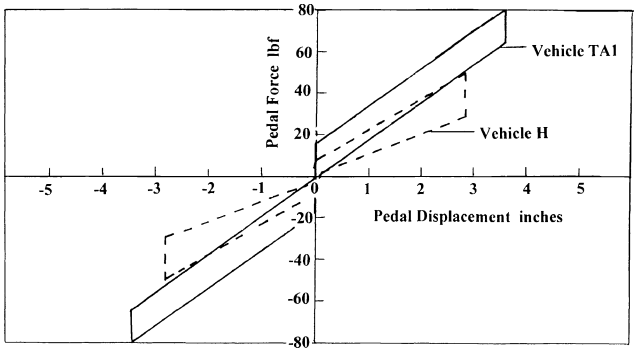

Fig. 21 Pedal force/feel characteristics between vehicles TA1 and H.

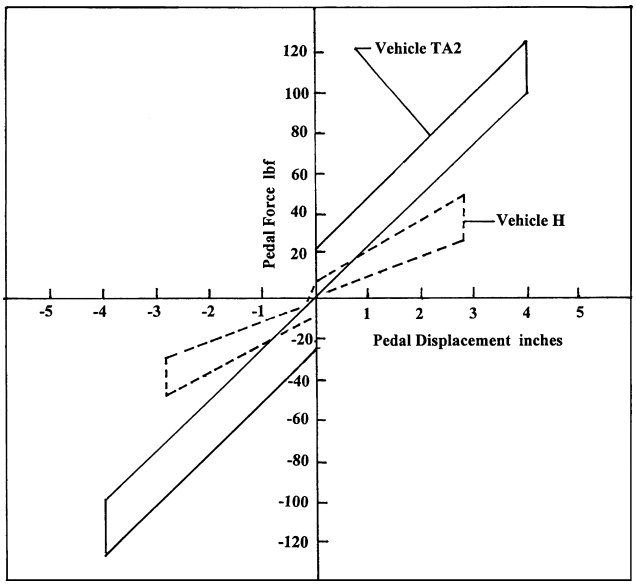

Fig. 22 Pedal force/feel system comparison between vehicles TA2 and H.

Figures 20–22 indicate significant differences between the pedal force/feel system on vehicle TA3 at 240 kn and those for the vehicles H, TA1, and TA2. For the reason stated in the preceding paragraph, the common system selected for comparison in each figure is that of vehicle H. The differences are summarized in Table 1. It is apparent from the graphs that the system for TA3 at 240 kn is significantly more nonlinear than those for the vehicles H, TA1, and TA2. The differences between the TA2 and TA3 force/feel characteristics are particularly noteworthy, not only for their force/displacement characteristics (compare the solid lines in Figs. 20 and 22) but also because these two aircraft are nearly identical in size, weight, and general aerodynamic configuration and have been produced by the same manufacturer.

The plots just discussed invite the following question: Can the "linearity" of the force/displacement characteristics of the control inceptor, in this case the pedals, serve as a useful metric for acceptability of these devices in tracking tasks? An example is in order at this point. The system in Fig. 23 represents a simplified pilot/vehicle system with a nonlinear force/feel system. Although the symbol for roll attitude (ϕ) has been identified as the system input and output, the symbol has been used merely for convenience here. That is, Fig. 23 represents any generic tracking task in which force/feel characteristics can be compared.

The "pilot" in Fig. 23 consists of a gain, a second-order transfer function modeling neuromuscular dynamics and a 0.2-s time delay. This pilot model is considerably simpler than the structural model of the pilot offered in the preceding analyses. The "vehicle" is a simple integrator with an adjustable control system gain. It can be easily shown that the open/loop pilot vehicle system obeys the dictates of the crossover model of the human pilot.[7] Two force/feel systems will be considered as shown in Fig. 24. These correspond approximately to the systems for TA3 and TA2 as shown in Figs. 20 and 22. They will be referred to here as simply system A and system B. In this simulation, each of these force/feel systems will be capable of the same maximum amplitude command to the integrator (vehicle model) through appropriate adjustment of the control system gain shown in Fig. 23 just before the integrator representing the vehicle dynamics.

A pulsive roll command will be provided in the simulation. The duration of the pulse will be 5 s. The units involved here are not important given the simplified nature of the simulation. Figures 25 and 26 show the responses for the systems with the two force/feel systems for the pilot gains $K_p = 1$, 2, 4, and 6. Figure 25 indicates that the responses of the high-sensitivity system A are much less

Table 1 Force/feel system summary

Vehicle	Ratio of max force to breakout force	Max force, lbf	Max displacement, in.
H	5.7	50	2.8
TA1	4.71	80	3.6
TA2	5.7	125	4.0
TA3[a]	1.45	32	1.3

[a]240-kn airspeed.

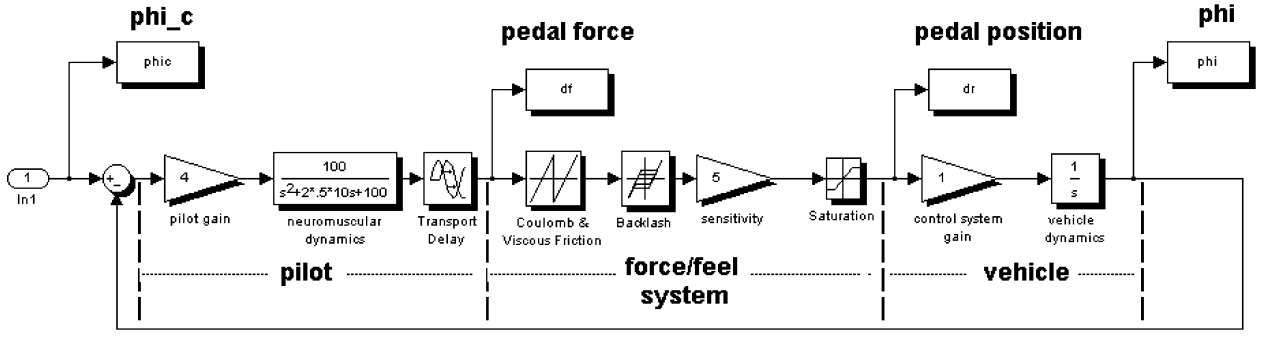

Fig. 23 Simplified computer model of a pilot/vehicle system.

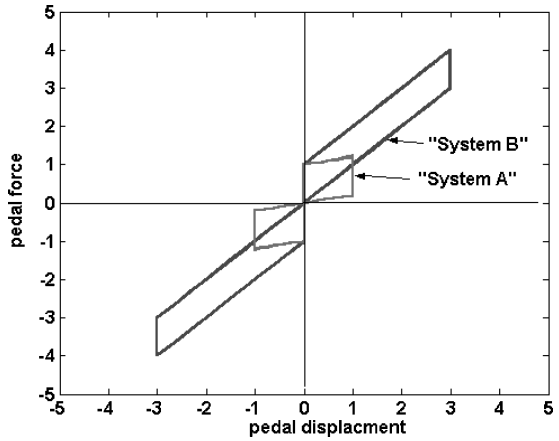

Fig. 24 Representations of the pedal force/feel systems A and B in the computer simulation of Fig. 23.

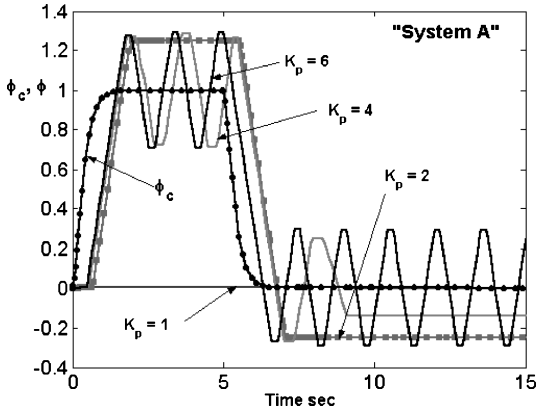

Fig. 25 Responses of the computer simulation of system of Fig. 23 for different pilot gains for the system A pedal force/feel system.

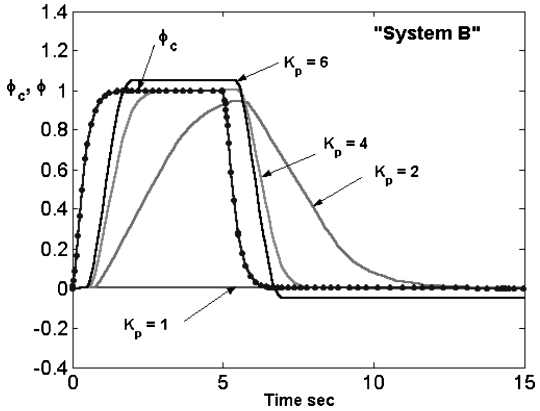

Fig. 26 Responses of the computer simulation of system of Fig. 23 for different pilot gains for the system B pedal force/feel system.

predictable and much more sensitive to the particular pilot gain chosen than those of system B shown in Fig. 26. Oscillations are apparent for all pilot gains at or above $K_p = 4$, whereas no such oscillations appear in Fig. 26 for system B. The inability of either system to respond with $K_p = 1$ is attributable to the fact that this gain value was not large enough to overcome the identical breakout forces in either force/feel system.

Figure 27 shows the plot of pedal force vs pedal displacement that occurred in the computer simulation just described with $K_p = 4$. It is interesting in that system A clearly shows that the pedal force associated with maximum pedal displacement has been exceeded. This has been identified as cable stretch in the figure, as it implies

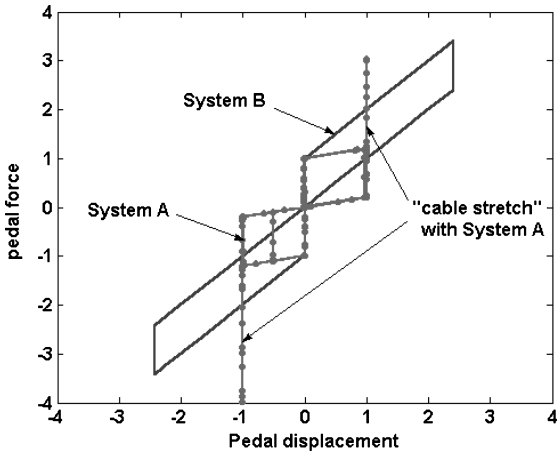

Fig. 27 Pedal force vs displacement for systems A and B in Fig. 23 for $K_p = 4$.

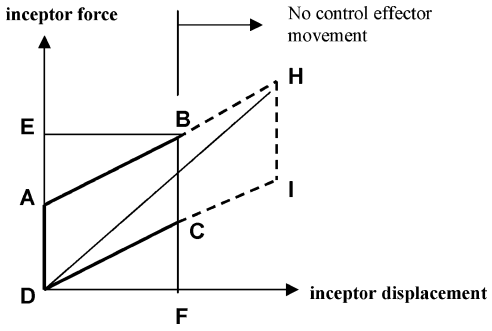

Fig. 28 Defining a linearity index.

forces exceeding that corresponding to the maximum deflection of the control surface in questtion. In an actual mechanical flight control system, of course, some pedal motion would be associated with this cable stretch. That is, the segments denoted as cable stretch would not be vertical, but would instead have large slopes consistent with large forces resulting in relatively small pedal motion. Again it is worth emphasizing that the maximum attainable control surface deflections for both systems A and B are identical.

In comparing results of the computer simulation just presented, the following must be emphasized: the two simulations have employed identical vehicle models, identical forms for the pilot models, identical pilot model gains, identical maximum control power, and identical command inputs. The nature of the vehicle responses were, however, very different. This fact that can be attributed solely to the different force/feel systems that have been modeled. Said another way, in terms of a closed-loop feedback structure that defines human pilot tracking behavior, there is a price to be paid for highly nonlinear force/feel characteristics. Such characteristics can produce unpredictable and unsatisfactory response characteristics in closed-loop control.

A simple way to quantify the linearity of a force/feel system is shown in Fig. 28. The heavy lines in Fig. 28 represent the full-throw force/feel characteristics for the inceptor in question. Figure 28 can be applied to a force/feel design in which inceptor forces beyond those associated with maximum control surface deflections are permitted, including allowing proportional pedal motion, but not allowing the larger control surface deflection associated with this increased pedal motion. Essentially, beyond a certain point, pedal motion would not be reflected in control surface motion (the dashed portion of the plot in Fig. 28). Point B is the point on the force/displacement graph farthest from the origin excluding the dashed lines. If the maximum inceptor force and displacement corresponds to maximum control effector displacement (as was the case in this study), points B and H are coincident. Based on Fig. 28, one

can propose a nondimensional linearity index (LI) as

$$\mathrm{LI} = 1 - \left[\frac{\mathrm{AREA(DAHD)} + \mathrm{AREA(DHID)}}{\mathrm{AREA(DEBF)}}\right] \tag{19}$$

Thus, if LI = 1 in Eq. (19), the force/feel system is completely linear. If LI = 0 (or possibly negative in the case when points B and H are not coincident), the system could be called highly nonlinear. Using the preceding metric, the LIs for the force/feel systems defined as systems A and B compare as follows: system A, LI $\cong$ 0.14; system B, LI $\cong$ 0.76. Accounting for the possibility of negative LI values in some applications, one can compare two LI results on a percentage basis as

$$\text{percentage difference} = \frac{|\mathrm{LI}_{\max} - \mathrm{LI}_{\min}|}{|\mathrm{LI}_{\min}|} \times 100 \tag{20}$$

where $\mathrm{LI}_{\max}$ and $\mathrm{LI}_{\min}$ refer, respectively, to the algebraically larger and smaller values of LI in the comparison. In this case, $\mathrm{LI}_{\max} = \mathrm{LI}_B$ and $\mathrm{LI}_{\min} = \mathrm{LI}_A$, and the percentage difference between the two is 443%.

Once a satisfactory breakout force has been determined in any force/feel system, the selection of the sensitivity of the system (or its reciprocal, the force gradient) can be based entirely on a desired value: the value of the LI. Obviously, one can create an inceptor force/feel system with an LI value near unity, which will prove unacceptable in use. This might involve inceptor force/feel characteristics with no breakout and with a range of applied forces that is far too small (or too large) for the particular human muscle group that is intended to create the forces with any accuracy. Thus, any criterion that might be developed based on some minimum value of LI should be regarded as a necessary but not sufficient condition for the acceptability of the force/feel system. It would appear that small LI values should nearly always be avoided in inceptors that can be used in closed-loop tracking by the human pilot. A low LI value almost invariably indicates an overly sensitive force/feel system in which the breakout and maximum inceptor forces at not sufficiently separated in magnitude.

V. Discussion

The research described in Secs. I–III used a simple dynamic model of the lateral/directional dynamics of a transport aircraft. A system survey of possible manual loop closures was presented. Using a structural model of the human pilot, two tracking tasks were examined, each with an eye toward capturing possible pilot/vehicle behavior than could occur in large roll upsets and in deliberate sideslip excursions. The pilot model was extended to emulate the effects of control sensitivity. The combined use of aileron and rudder for roll-attitude tracking was shown to exhibit poor performance and stability as compared to aileron-alone inputs. In addition, it was suggested that pedal force/feel systems with large sensitivities (low force gradients) could precipitate lateral/directional pilot-induced oscillations with such combined strategies caused by the large lateral accelerations at the pilot's station that occurred. A sideslip capture task also suggested that large sensitivities in the rudder control system could lead to large lateral accelerations at the pilot's station and serve as a PIO trigger. Although simplified in nature, the analytical study emphasized the handling qualities and performance issues that can arise in continuous use of rudder inputs in flight control tasks. In Sec. IV, a limited comparison of pedal force/feel systems for four aircraft was undertaken. It was shown that these systems can differ significantly in sensitivity and linearity. A computer simulation of a simplified pilot/vehicle system showed that highly sensitive and nonlinear force/feel characteristics can adversely affect response predictability. A linearity index was introduced to quantify the linearity of any force/feel system. It would be of interest to determine the manner in which numerical values of this index would map into handling qualities ratings for specific tasks.

VI. Conclusions

An analytical study has been conducted to investigate the handling qualities and performance implications of rudder control strategies and systems in transport aircraft. The study focused on the dynamics of a single, representative, transport aircraft, a dynamic model of which is readily available in the literature. In addition, a limited comparison of force/feel characteristics of four aircraft was undertaken. Based on this study, the following conclusions can be drawn:

1) A system survey of possible manual loop closures that could be employed by the pilot using rudder control led to the identification of two tracking strategies that could occur in large roll upsets and deliberate sideslip excursions. These strategies involved the combined and separate use of aileron and rudder inputs.

2) The analysis suggested that pedal force/feel systems with large sensitivities (or equivalently, low force gradients) could precipitate pilot-induced oscillations when combined aileron and rudder inputs were employed in roll maneuvers or when separate aileron and rudder inputs were employed in wings-level sideslip capture tasks. In each case, this susceptibility could be attributed to large lateral accelerations occurring at the pilot's station.

3) The analysis suggested that wings-level sideslip captures might serve as a useful pilot-in-the-loop flight simulation task to investigate handling qualities issues involving rudder control.

4) The pedal force/feel systems for a helicopter and two transport aircraft were compared and found to be significantly more linear in their force/displacement characteristics than that of a third comparison transport aircraft. A simple computer simulation modeling a piloted, closed-loop tracking task clearly demonstrated that highly nonlinear force/feel systems can produce poor response predictability and tracking performance as compared to more linear force/feel designs.

5) A simple index can be used to quantify the linearity of force/feel systems. Systems with small index values will exhibit high sensitivity (low force gradients) and will likely produce unpredictable vehicle responses in closed-loop tracking tasks. The manner in which the index affects perceived vehicle handling qualities remains a research issue.

Acknowledgments

The research reported herein was supported by a grant from the Federal Aviation Administration, through the William J. Hughes Technical Center, Atlantic City International Airport, New Jersey. The Grant Technical Manager is Robert McGuire. The conclusions drawn in this study are those of the author and do not necessarily reflect those of the Federal Aviation Administration.

References

[1]Dornheim, M. A., "Did Rudder Motions Snap Off A300 Fin?," *Aviation Week and Space Technology*, Vol. 156, No. 3, 21 Jan. 2002, pp. 24–26.

[2]Dornheim, M. A., "Crash Probe Triggers Rudder Design Scrutiny," *Aviation Week and Space Technology*, Vol. 156, No. 13, 1 April 2002, pp. 44–46.

[3]Dornheim, M. A., "Flight 587 Probe Shows Tails Have Been Overloaded Before," *Aviation Week and Space Technology*, Vol. 157, No. 22, 25 Nov. 2002, pp. 44, 49–51.

[4]Fiorino, Frances, "Upset Events, Wake Vortices at Center of Flight 587 Probe," *Aviation Week and Space Technology*, Vol. 156, No. 16, 22 April 2002, p. 39.

[5]McRuer, D., Ashkenas, I., and Graham, D., *Aircraft Dynamics and Automatic Control*, Princeton Univ. Press, Princeton, NJ, 1973.

[6]Stapleford, R. L., McRuer, D. T., and Magdaleno, R. E., "Pilot Describing Function Measurements in a Multiloop Task," *IEEE Transactions on Human Factors in Electronics*, Vol. HFE-8, No. 2, 1967, pp. 113–124.

[7]Hess, R. A., "Feedback Control Models—Manual Control and Tracking," *Handbook of Human Factors and Ergonomics*, edited by G. Salvendy, Wiley, New York, 1997, Chap. 38.

[8]Hess, R. A., "Unified Theory for Aircraft Handling Qualities and Adverse Aircraft-Pilot Coupling," *Journal of Guidance, Control, and Dynamics*, Vol. 20, No. 6, 1997, pp. 1141–1148.

[9]Graham, D., and McRuer, D., *Analysis of Nonlinear Control Systems*, Dover, New York, 1961, p. 228.

[10]McRuer, D. T., Magdaleno, R. E., and Moore, G. P., "A Neuromuscular Actuation System Model," *IEEE Transactions on Man-Machine Systems*, Vol. MMS-9, No. 3, 1968, pp. 61–71.

[11]Hess, R. A., "An Inquiry into Whether a Pilot-Induced Oscillation Was a Factor in the Crash of American Airlines Flight 587," Document 288388, Rept. submitted to the National Transportation Safety Board, Washington, DC, Dec. 2003.

[12]Gibson, J. C., and Hess, R. A., "Stick and Feel System Design," AGARDograph 332, March 1997.

[13]"STEADES—Safety Trend Evaluation, Analysis & Data Exchange System," Transport Category Airplane Rudder and Lateral Control Events, International Air Transport Association (IATA), First Interim Rept., Dec. 2002.

[14]*Aviation Safety and Pilot Control—Understanding and Preventing Unfavorable Pilot-Vehicle Interactions*, National Academy Press, Washington, DC, 1997, Chap. 5.

[15]Heffley, R. K., Hess, R. A., and Zeyada, Y., "Computer Modeling and Simulation for Helicopter Pilotage Task Analysis," U.S. Army Aviation and Missile Command, Research, Development and Engineering Center, USAAMCOM TR 02-D16, Huntsville, AL, June 2000.

[16]"Aeronautical Design Standard, Performance Specification Handling Qualities Requirements for Military Rotorcraft, ADS-33E-PRF," U.S. Army Aviation and Missile Command, Huntsville, AL, March 2000.